Molecular Model of the $\alpha_{IIb}\beta_3$ Integrin

Bradley P. Feuston,*,† J. Christopher Culberson,† and George D. Hartman‡

Departments of Molecular Systems and Medicinal Chemistry, Merck Research Laboratories, West Point, Pennsylvania 19486

Received April 1, 2003

A molecular model of the $\alpha_{IIb}\beta_3$ integrin has been developed utilizing (i) the crystal structure of $\alpha_v\beta_3$, (ii) homology model of the α_{IIb} subdomain, and (iii) the docking of $\alpha_{IIb}\beta_3/\alpha_v\beta_3$ dual and selective inhibitors into the putative binding sites of $\alpha_{IIb}\beta_3$ and $\alpha_v\beta_3$. Since the binding sites of these integrins are located at the interface between the two heads of the individual subunits, only the $\alpha_{IIb}\beta_3$ head region is modeled. The 3D conformations of two loops in α_{IIb}, whose residues have been implicated in non-peptide ligand binding, could not be determined from homology with α_v alone. Mutagenesis data and the modeling of small ligand binding contributed to the rational design of these loop conformations. The final energy minimized loop conformations exhibit permissible ϕ/ψ angles and contribute to a binding site model of $\alpha_{IIb}\beta_3$ that is consistent with both the known mutagenesis studies and in-house structure−activity relationships. The charged residues α_{IIb}:E117 and β_3:R214 are found to dominate the ligand−protein binding interaction. The previously identified "exosite" is also identified as a hydrogen bond, hydrophobic or $\pi-\pi$ interaction with Y190, similar to the recently proposed binding model of $\alpha_v\beta_3$.

Introduction

Integrins are members of a superfamily of cell surface glycoproteins pivotal in cell−cell and cell−extracellular matrix adhesion. As heterodimeric proteins, integrins are composed of two subunits generally referred to as α and β. There have been 19 α and 8 β subunits identified, although only a relatively small number of unique combinations have been observed. Since integrins play such a crucial role in cell adhesion they are considered pharmaceutical targets in a number of therapeutic areas, e.g., cancer, macular degeneration, arthritis, and osteoporosis.[1−4] However, the only approved anti-integrin therapy targets the blood platelet specific integrin $\alpha_{IIb}\beta_3$.[3] The $\alpha_{IIb}\beta_3$ integrin has also been studied extensively as the prototypical integrin.

There have been numerous studies on the structure of the integrins over the past 20 years. Although there has been some success in determining the gross structure of the heterodimer, only the atomic-level structure of $\alpha_v\beta_3$ has been characterized through X-ray diffraction and made publicly available. Integrins are transmembrane proteins expressed in surface membranes as heterodimers. The gross shape and dimensions of the integrins' extracellular structure as determined by electron microscopy and cryomicroscopy are best characterized as a large head region supported by a long thin tail extending into the transmembrane region.[5,6] The putative binding site is formed by the coming together of the heads of the α and β subunits. The head of the α subunits features the so-called β propeller motif, seven homologous blades packed in a cylindrical fan shape, and the ∼200 residue "inserted" domain, homologous to the A domain of the von Willebrand factor.[7] The metal-ion-dependent-adhesion-site (MIDAS) is an important feature of this domain as determined from the crystal structures of the A domains (αA) of several integrins.[8] However, the existence of a MIDAS motif in β_3 was predicted from a naturally occurring mutation of Y119D in $\alpha_{IIb}\beta_3$ integrin that resulted in abnormal ligand and cation binding functions.[9] Xiong et al. identified such a MIDAS motif in the βA domain of the β_3 subunit when they determined the crystal structure of the extracellular segment of $\alpha_v\beta_3$ integrin in the presence of Ca^{2+}.[10]

Similar to $\alpha_v\beta_3$ and a number of other integrins, the platelet specific integrin, $\alpha_{IIb}\beta_3$, is known to bind an Arg-Gly-Asp (RGD) segment in peptides including fibrinogen, echistatin, and vitronectin.[11] For this reason, a number of non-peptide RGD mimetics have been synthesized and investigated for integrin binding. This laboratory has previously reported on the design of RGD mimetics as potential antithrombotic ligands targeting the fibrinogen receptor, $\alpha_{IIb}\beta_3$ integrin.[12−14] In general, $\alpha_{IIb}\beta_3$ and $\alpha_v\beta_3$ antagonists are characterized as zwitterionic structures that retain the α-carboxylic acid of aspartic acid and a basic moiety that mimics the arginyl guanidine present in the RGD triad. With the availability of the crystal structure of $\alpha_v\beta_3$ integrin,[10] it became possible to model the binding of small-molecule ligands to $\alpha_v\beta_3$. Molecular modeling in this laboratory identified important protein contacts for four different chemical classes of non-peptide ligands bound to the putative binding site of $\alpha_v\beta_3$.[15] These included contacts in both the α and β subunits as well as the identification of the "exosite" interaction.[12] Consistent with the known SAR, it was found that the basic nitrogen of the ligand interacts with α_v:D150, while the ligand's acid component interacts with β_3:R214. In addition, an unexpected finding of $\pi-\pi$ stacking interaction for the "exosite substituent" with Y178 of α_v correlated with increased potency and specificity for $\alpha_v\beta_3$.[14,15]

Efforts to identify selective integrin antagonists in this laboratory have resulted in the synthesis of a number of both selective and dual antagonists of the

* To whom correspondence should be addressed. Tel: (215) 652−5048. Fax: (215) 652−4625. E-mail: bradley_feuston@merck.com.
† Department of Molecular Systems.
‡ Department of Medicinal Chemistry.

10.1021/jm030146j CCC: $25.00
Published on Web 10/30/2003

Figure 1. MOE alignment results of the α_{IIb} and α_v sequences. The red residues in α_v correspond to the known active site. The red and blue residues for the α_{IIb} sequence indicate residues that do and do not affect binding when mutated, respectively. The residues in bold are found play a crucial role in small ligand binding from the respective binding models, $\alpha_{IIb}\beta_3$ or $\alpha_v\beta_3$.

$\alpha_{IIb}\beta_3$ and $\alpha_v\beta_3$ receptors.[16−19] The combination of this in-house SAR with the crystal structure of $\alpha_v\beta_3$ provided the impetus for the rational design of an $\alpha_{IIb}\beta_3$ model. An accurate model of the $\alpha_{IIb}\beta_3$ integrin would be a valuable tool in the design and optimization of high-affinity drug-like ligands specific for this receptor.

Construction of the $\alpha_{IIb}\beta_3$ Model

To obtain a preliminary $\alpha_{IIb}\beta_3$ model, the crystal structure of the β_3 subunit from the $\alpha_v\beta_3$ crystal structure was simply combined with a homology model for α_{IIb}, obtained from α_v. A theoretical model of α_{IIb} is available from the Protein DataBank (PDB ID: 1JX5).[21] However, the 3D alignment of the model with the α_v subunit resulted in unreasonable $\alpha_{IIb}\beta_3$ contacts and was not pursued further. Since the putative binding site is located in the contact region between the heads of both subunits, the tails of both subunits are ignored in the present model. A homology model for α_{IIb} was obtained using the MOE modeling software package[22] with the crystal structure of the α_v subunit extracted from the $\alpha_v\beta_3$ crystal structure[10] and the sequences of α_{IIb} (P08514) and α_v (P06756).[21] These α subunits are highly homologous with 38% identity, 54% homology, and only 5% gaps, as seen in Figure 1. The sequence numbering for α_v and α_{IIb} has been adopted from refs 10 and 21, respectively. Since MOE did not accommodate simultaneous relaxation of multiple subunits, no attempt was made to optimize the structure with MOE. The MOE model was obtained through Cartesian averaging over 10 intermediate models. In Figure 1, the α_v residues depicted in red correspond to the putative binding region. For α_{IIb}, the residues that affect ligand binding when mutated are shown in red, while those whose mutations do not affect ligand binding are shown in blue.[21] It is apparent from Figure 1 that there are two segments of the sequence in the binding region for which α_{IIb} contains additional residues, one with eight extra residues and the other with three additional residues. It is not clear what role these residues may play in small ligand binding, but it is clear that their conformation cannot be determined from the homology model, especially since the residues on either side of the gaps also fail to be homologous to α_v. Therefore, two segments have been identified whose conformations are indeterminate from the homology model. These 17 and 12 residue segments, defined in Table 1, are shown in italics in Figure 1 and labeled as Loop 1 and Loop 2, respectively. Since the regions on either side of these defined loops have high homology with $\alpha_v\beta_3$, the MOE homology model for atoms in the main peptide chain was retained in the present model of the $\alpha_{IIb}\beta_3$ heterodimer. These unspecified segments have also not been observed in any of the crystallized proteins available from the Protein Data Bank. Both Loop 1 and Loop 2 are of special importance since they contain segments of conserved residues, whose mutations destroy activity. In particular, Loop 1 has several acidic residues that may align well with the aspartic acids α_v:D148/D150, which contributes to the small-ligand binding site in the $\alpha_v\beta_3$ model as seen from the sequence alignment in Figure 1 (see ref 15).

Because the homology model was obtained in the absence of β_3, there were many close contacts between the α_{IIb} and β_3 side-chains in the preliminary model. Minimizing the α_{IIb} side-chain atoms in the presence of β_3 would eliminate these close contacts. To accomplish this task, a model of the interface was constructed since it is unnecessary to consider all 12 722 atoms in the $\alpha_{IIb}\beta_3$ model. All α_{IIb} atoms within 10 Å of the β_3 subunit and all atoms in β_3 within 5 Å of the α_{IIb} subunit were isolated to form the interface model. Only the α_{IIb} side-chain atoms within 5 Å of β_3 were subsequently minimized. This 5 Å layer of movable atoms sandwiched between two 5 Å regions of fixed atoms ensured that the relaxed interface could be trivially incorporated back into the full model while allowing a sufficiently large

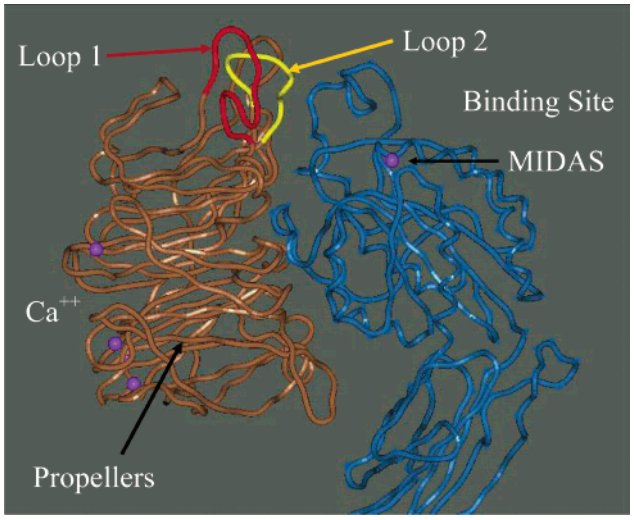

Figure 2. Preliminary model obtained with the MOE homology and relaxation of the $\alpha_{IIb}\beta_3$ interface, α_{IIb} in brown and β_3 in blue. Loop 1 and Loop 2 are shown in red and yellow, respectively. Calcium cations are depicted in purple. The MIDAS region of β_3 is also indicated.

region to be optimized. Energy minimization was performed with the Merck molecular force field (MMFFs) within BATCHMIN, employing a distance-dependent dielectric constant of 4r/Å.[22,23] After suitable conformations were obtained for Loop 1 and Loop 2 (see below), the β_3 side-chain atoms within 5 Å of the α_{IIb} subunit were also energy minimized in a similar manner while the remaining β_3 atoms and the model α_{IIb} subunit were held fixed.

The structure of $\alpha_{IIb}\beta_3$ obtained from the interface minimization procedure described above served as the initial state for modeling the loops and is shown in Figure 2, where the brown and blue pipes correspond to α_{IIb} and β_3 subunits, respectively. Also depicted in Figure 2 are the Ca^{2+} ions (purple), Loop 1 (red in foreground), and Loop 2 (yellow). The loop conformations shown in Figure 1 were the direct result of the MOE homology-modeling program and the subsequent relaxation of the $\alpha_{IIb}-\beta_3$ interface. As well as containing residues crucial for ligand binding, these loops may play a prominent role in the interface between the two subunits, as can be seen in Figure 2. In the absence of any structural information concerning these loops there is little guidance as to the most likely conformations that these loops will adopt. However, utilizing the previously published binding model for $\alpha_v\beta_3$, specific compounds that are known to be selective for $\alpha_{IIb}\beta_3$ or $\alpha_v\beta_3$ and dual antagonists, i.e., compounds that bind to both receptors, a model for these loops of $\alpha_{IIb}\beta_3$ may be rationally designed. The general procedure employed here involves generating a loop that is minimized in the presence of the remaining protein atoms followed by docking of the ligands. The success of the docking results with low-energy loop conformations to explain the observed selectivity was the basis for the choice of the final structure. A large number of iterations of loop conformation generation and docking studies were performed. Each candidate conformation was eliminated as early as possible in the docking study by considering first an $\alpha_{IIb}\beta_3$ selective ligand and then an $\alpha_v\beta_3$ selective ligand.

The ligands utilized in the present work are depicted in Figure 3.[16−20] The PLAGGIN and SPAV3 results, specific assays for $\alpha_{IIb}\beta_3$ and $\alpha_v\beta_3$ binding, respectively, are given in Table 2. The efficacy of these compounds to inhibit $\alpha_{IIb}\beta_3$ was tested in the platelet aggregation (PLAGGIN assay).[16] The affinities of these compounds for the $\alpha_v\beta_3$ receptor were determined by a scintillation proximity bead-based binding assay using ^{125}I-labeled **5** as the ligand.[16] In this $\alpha_v\beta_3$ scintillation proximity assay (SPAV3), the $\alpha_v\beta_3$ integrin was purified from HEK 293 cells overexpressing human recombinant $\alpha_v\beta_3$. Yamamoto et al. describes this method for purification of $\alpha_v\beta_3$ from human placentae.[25] The assay utilizes lyophilized wheat germ agglutinin scintillation proximity beads and has been previously described in detail.[16]

Compounds **1**−**3**, sulfonamide class compounds, are all specific inhibitors of $\alpha_{IIb}\beta_3$. Compound **2** is tirofiban hydrochloride, a marketed platelet aggregation inhibitor. Compound **4**, also a sulfonamide, is a dual inhibitor, while **5**−**8** are selective inhibitors of $\alpha_v\beta_3$.[18] Compound **7** is also the $\alpha_v\beta_3$ antagonist reported by GlaxoSmithKline as SB 273005, while **8** is considered a chain-shortened $\alpha_v\beta_3$ antagonist.[20,26] Compound **9**, although containing the generic $\alpha_{IIb}\beta_3$ pharmacophore, i.e., a positive and negatively charged moieties separated by ~12 bonds, is ineffective against either integrin.

Modeling the Loops

Since there are a large number of possible loop conformations that would be energetically favorable, the conformation that was most consistent with observed structure−activity relationships (SAR) was retained. In Figure 3, there are 12−15 bonds separating the carboxylic carbon from the charged nitrogen in the $\alpha_{IIb}\beta_3$ selective inhibitors, **1**−**3**, whereas for $\alpha_v\beta_3$ selective compounds, **5**−**8**, the corresponding distance ranges from 9 to 12 bonds. For this reason, it is postulated that the distance between the complementary charge groups of the protein are farther apart in $\alpha_{IIb}\beta_3$ than in $\alpha_v\beta_3$.[16] In the previously published binding model for $\alpha_v\beta_3$, the residues β_3:R214 and α_v:D148/D150/Y178 played a role in non-peptide ligand binding.[15] The distances in the crystal structure of $\alpha_v\beta_3$ between the charged nitrogen of β_3:R214 and the carboxylic carbons α_v:D150 and α_v:D148 are 12.9 and 12.0 Å, respectively. The homology model shown in Figure 2 places α_{IIb}:D159 and α_{IIb}:E157 in a similar relationship to each other and to β_3:R214 as are D150, D148, and R214 in $\alpha_v\beta_3$. The distances between β_3:R214 and acids α_{IIb}:D159 and α_{IIb}:E157 in the preliminary $\alpha_{IIb}\beta_3$ model are 15.1 and 10.1 Å, respectively. However, this $\alpha_{IIb}\beta_3$ model positions α_{IIb}:D159 such that α_{IIb}:Y190 blocks any conformation of an active ligand from making contacts at α_{IIb}:D159 and β_3:R214 simultaneously. Therefore, docking studies (see binding model below) with this Loop 1 conformation result in the ligand's basic nitrogen interacting with α_{IIb}:E157 at much too short a distance for an extended ligand conformation even for the $\alpha_v\beta_3$ specific ligands. In addition, recent mutagenesis studies indicate that neither α_{IIb}:D159 nor α_{IIb}:E157 are required for ligand binding (see Figure 1).[21] However, an aspartic acid α_{IIb}:D163 in Loop 1 was identified by mutagenesis as crucial for ligand binding, although it was inaccessible to ligands in the MOE model. Therefore, this initial $\alpha_{IIb}\beta_3$

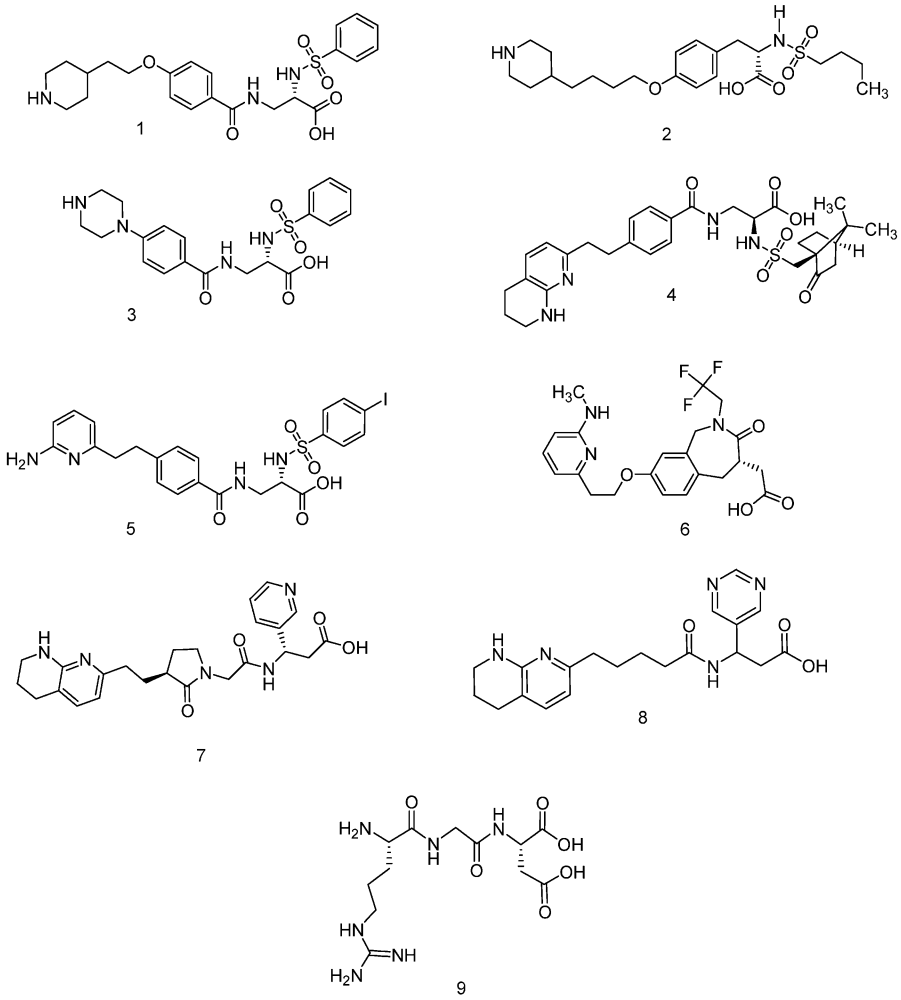

Figure 3. The nine nonpeptide ligands used in the binding model. Compounds **1**−**3** are $\alpha_{IIb}\beta_3$ selective antagonist, **4** is a dual antagonist, **5**−**8** are selective for $\alpha_v\beta_3$, and **9** is inactive in both integrins.

Table 1. Residues Defining Loop 1 and Loop 2

loop	residues count	sequence	residue range
1	17	NTLSRIYVENDFSWDKR	149−165
2	12	NVLEKTEEAEKT	114−125

Table 2. Binding Assay Results for **1**−**9**

	IC_{50} (nM)	
molecule	PLAGGIN	SPAV3
1[a]	10[a]	>1000[a]
2[b]	15[b]	>1000[c]
3[c]	16[c]	>1000[c]
4[d]	157[c]	0.11[c]
5[a]	1600[a]	0.08[a]
6[e]	>10 000[e]	0.15[e]
7[f]	>10 000[f]	0.35[f]
8[g]	>10 000[g]	3.3[g]
9[f]	>10 000[f]	>10 000[f]

[a] Ref 16. [b] Ref 14. [c] Previously unpublished. [d] Ref 19. [e] Ref 15. [f] Ref 17. [g] Ref 20.

model was eliminated from further consideration because it was inconsistent with both mutagenesis studies and known SAR.

New models for $\alpha_{IIb}\beta_3$ were generated from the homology model by sampling conformations of Loop 1 and Loop 2. As an integral part of the putative binding site for $\alpha_{IIb}\beta_3$, the loops were modeled in the presence of the crystallographically determined β_3 subunit. Initially, only Loop 1 was considered crucial for binding since the corresponding region of Loop 2 in $\alpha_v\beta_3$ did not play a role in non-peptide ligand binding. Hence, Loop 2 was held fixed as in the preliminary model, while Loop 1 was modified by hand. A number of conformations were generated and then energy minimized in the presence of the remaining protein atoms. The conformations were chosen to allow favorable ligand interactions with α_{IIb}:D163 and to minimize interactions with the other Loop 1 acidic residues. The model for these minimization procedures was obtained by selecting all atoms within 10.0 Å of any atom in Loop 1, i.e., residues α_{IIb}:149−165, in both the α_{IIb} and β_3 subunits. These atoms surrounding the loop were held fixed, while the atoms in the loop were optimized. The procedure was repeated many times for Loop 1 utilizing acceptable ϕ/ψ angles and small-molecule binding as acceptance criteria. No ligands were present during optimization of the loops.

Binding Model

The compounds in Figure 3 were selected to best discriminate between possible selective binding models for $\alpha_{IIb}\beta_3$. Compound **1** served as the prototypical $\alpha_{IIb}\beta_3$ selective ligand, while **7** served as the counterexample for any $\alpha_{IIb}\beta_3$ binding models. Multiple conformations of **1** were calculated using Merck's in-house knowledge-

Table 3. Residues that Define the Binding Site[a]

subunit	total residue count	residues in binding site
α_{IIb}	58	109, 113, 115, 144−158, 177−184, 191−200, 217−225, 243−244, 246, 256−265, 290, 294
β_3	83	118−128, 156−189, 211−222, 248−256, 259, 262−263, 289, 310−314, 317−318, 321, 333−337, Ca++

[a] Residues within 15 Å of the bound conformation of **1.**

based conformation generator *et*.[27] Each conformation was placed in the putative binding site. The binding site was initially defined as having the selective ligand making favorable interactions with α_{IIb}:D163 and β_3:R214, where the α_{IIb}:D163 position was determined by the Loop 1 conformation. Acceptable binding modes allow the selective ligand to adopt an extended conformation while making the desired protein contacts. To construct a model suitable for energy minimization of the ligand, an extended conformation of **1** was hand-docked in a reasonable binding orientation. Protein atoms within 15.0 Å of the ligand were then identified as the binding site. The ligand, formally charged as the zwitterion, was energy minimized in this binding site using the MMFFs force field in BATCHMIN with a dielectric constant of 1.0. Protein atoms, including the loop atoms, were held fixed. If this procedure resulted in a reasonable binding model for **1**, the process was repeated for **7**. Since, in this case, the objective was to rule out a successful binding model for **7**, many more attempts were required to ensure that possible binding modes had been thoroughly tested. To evaluate the internal strain of the bound conformation induced by the ligand−protein interactions, a maximum of 350 conformations were generated and minimized for each molecule. The initial conformations, generated by *et*, were chosen to be diverse by requiring that no two conformations differed by less than 0.6 Å RMSD. Energy minimization of these conformations was performed for the neutral molecule using the 4r distance-dependent dielectric constant, since energy minimization of the fully charged ligand in vacuo would bring the two charged ends together to form a cupped conformation. The closest in vacuo optimized structure was identified for each of the bound conformation to ascertain the degree of protein induced conformational distortion. Using multiple initial conformations combined with manual rotation of torsion angles to overcome local minima, the docking procedure was repeated many times for each of the ligands in an attempt to find a ligand conformation with the least internal strain and the best protein−ligand binding interactions. Both in house and third party docking software were initially examined in the previous study on $\alpha_v\beta_3$. It was found that the resulting docked conformations were dominated by hydrophobic and van der Waals interactions. Since the results of these automated docking procedures were inconsistent with mutagenicity data and known SAR, the hand-docking procedure described above was employed.

During this procedure for Loop 1, it became apparent that many of the binding models involved favorable contacts with α_{IIb}:E117 in Loop 2. In the previously discussed mutagenesis study of the $\alpha_{IIb}\beta_3$ integrin, the authors discovered that while α_{IIb}:D163 was important to ligand binding, mutations of α_{IIb}:E117 also resulted in loss of ligand binding.[21] This information required that alternative conformations of Loop 2 also be evaluated. Utilizing the best Loop 1 conformation, many Loop 2 conformations were also generated and energy minimized in a manner similar to the Loop 1 conformation search. For this case, the binding site was defined as having the selective ligand making favorable interactions with α_{IIb}:E117 and β_3:R214, where the α_{IIb}:E117 position was determined by the Loop 2 conformation. When satisfactory loop conformations were obtained individually for Loop1 and Loop 2, they were both minimized simultaneously. Finally, as described previously, the β_3 side-chain atoms within 5 Å of the α_{IIb} subunit were relaxed in the presence of α_{IIb} model to complete the $\alpha_{IIb}\beta_3$ heterodimeric model. Although there was minimal change in the protein atom positions during these last two optimization steps, all the ligands were minimized for the last time in the final $\alpha_{IIb}\beta_3$ model. The protein atoms comprising the active site were redefined using the best binding mode of **1** identified as discussed above. Insignificant changes of the bound conformation occurred when **1** was minimized in this redefined site. The binding site defined for **1** was then utilized for the remaining ligands. The residues that define the binding site are given in Table 3. While all of Loop 2 residues contribute to the binding site, only the ends of Loop 1 play a role. The β_3 subunit also contributes nearly twice as many residues to the binding site as α_{IIb}, although there are more ligand interactions with the α_{IIb} subunit as presented below.

To better ascertain the stability of the minimized ligand−protein complex, both the ligand and the protein side-chain atoms in the binding site were allowed to relax in the final analysis. Starting from the best binding mode for each of the ligands in the rigid crystal structure, the side-chain atoms of the protein within 5 Å of the ligand were permitted to relax along with the ligand. In this final energy minimization procedure, all the protein backbone atoms and the side-chain atoms beyond 5 Å of the docked ligand remained in fixed positions. The root-mean-square deviation (RMSD) between the side-chains before versus after relaxation was typically small (∼0.25 Å) for all the molecules. The only exception to this finding is **5**, whose side-chain RMSD was 0.44 Å.

Results

The Ramachandran plots of Loop 1 and Loop 2 are shown in Figures 4 and 5, respectively. These plots demonstrate that the ϕ/ψ angles of the loops are consistent with the allowed values with only a few exceptions. The ϕ/ψ angle distribution for the $\alpha_{IIb}\beta_3$ model is also found to be comparable to the $\alpha_v\beta_3$ crystal structure ϕ/ψ angle distribution as seen by comparing the Ramachandran plots of these two integrins, $\alpha_{IIb}\beta_3$ in Figure 6 and $\alpha_v\beta_3$ in Figure 7. Only the head region of the $\alpha_v\beta_3$ crystal structure is included in this analysis similarly to the $\alpha_{IIb}\beta_3$ model. The final $\alpha_{IIb}\beta_3$ model is shown in Figure 8, where Loop 1 (red) and Loop 2 (yellow) are highlighted on the α_{IIb} subunit (brown) with

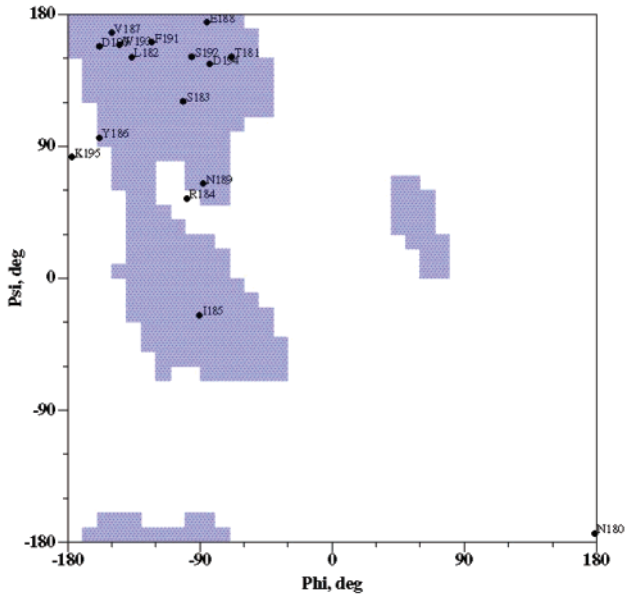

Figure 4. Ramachandran plot for Loop 1.

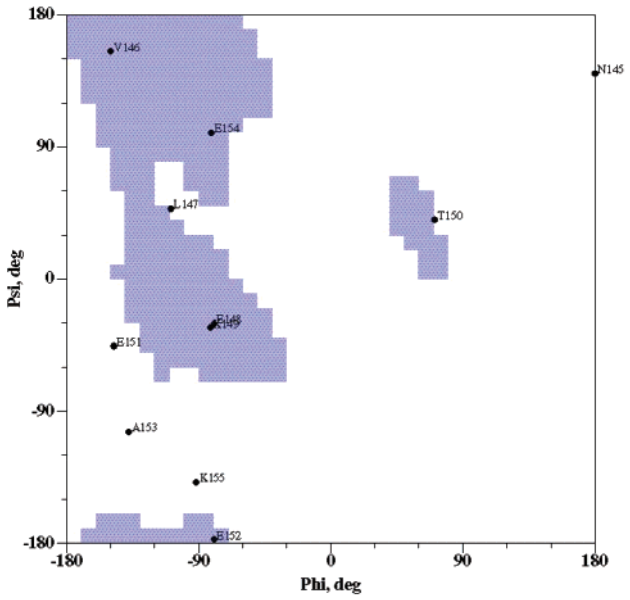

Figure 5. Ramachandran plot for Loop 2.

β_3 in blue. The best model for $\alpha_{IIb}\beta_3$ resulted in an active site defined by binding interactions with the three key residues, α_{IIb}:E117, α_{IIb}:Y190, and β_3:R214. For reference, these three $\alpha_{IIb}\beta_3$ residues and the corresponding $\alpha_v\beta_3$ residues are shown in bold in Figure 1. An overlay of the $\alpha_{IIb}\beta_3$ and $\alpha_v\beta_3$ model binding sites is depicted in Figure 9 with α_{IIb} in yellow and α_v in red. As can be seen in Figure 9, the $\alpha_{IIb}\beta_3$ site is very similar to the $\alpha_v\beta_3$ site, although with larger distances between the arginine in the β (blue) subunit and the acids in the α subunit. The "exosite" contact in both models is found to be a favorable interaction with the displayed tyrosine. The critical distance between the charged residues in the binding model for $\alpha_{IIb}\beta_3$ is 15.3 Å (α_{IIb}:E117-β_3:R214) and 12.9 Å (α_{IIb}:D150-β_3:R214) in $\alpha_v\beta_3$, thus providing a plausible explanation for the observed differences in ligand assay results, Table 2. The bound conformations of **1**−**9** are presented in Figures 10−18, respectively. Recall that **1**−**3** are selective $\alpha_{IIb}\beta_3$ antagonists, **4** is a dual antagonist, **5**−**8** are specific $\alpha_v\beta_3$ antagonists, and

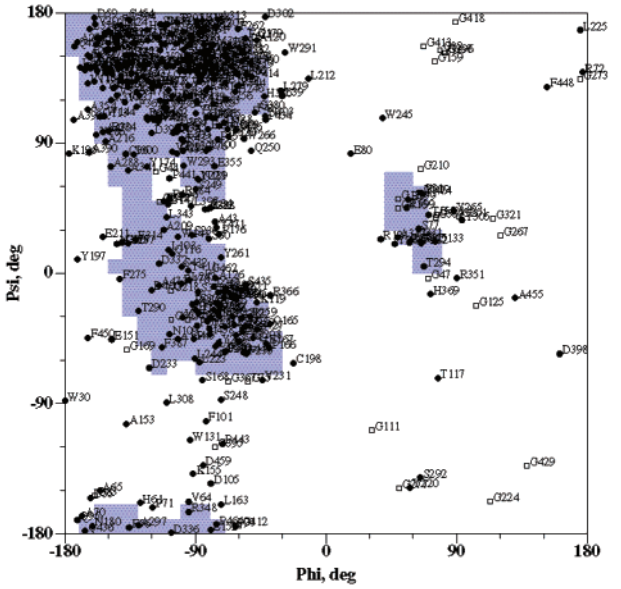

Figure 6. Ramachandran plot for the present $\alpha_{IIb}\beta_3$ model.

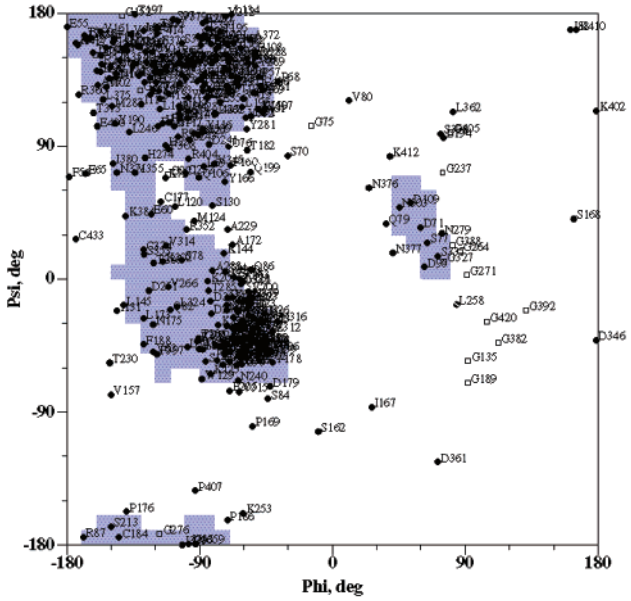

Figure 7. Ramachandran plot head region of $\alpha_v\beta_3$ determined by X-ray diffraction, obtained from PDB ID: 1JV2.

9 is inactive for both integrins. As can be seen in these figures, the charged ends of the selective ligands, **1**−**3**, make good contact with the protein at the appropriate distance and orientation, while the nonbinders, **5**−**9**, generally do not. In addition, a favorable interaction is made between the selective ligands and Y190, the interaction discovered in this laboratory and referred to as the exosite.[12,14] The notable exception to the rigid binding model is the fairly inflexible compound **6**, which appears to make good charge interactions but only a very weak hydrogen bond with the exosite tyrosine. However, upon relaxation of both the side-chain atoms and the ligands, **6** loses the additional exosite interaction completely.

A summary of these binding results for **1**−**9** are given in Tables 4 and 5. In Table 4, the RMSDs between the ligands in both the rigid binding site (RBS) and flexible binding site (FBS) and the closest in vacuo minimum (E_0) for the neutral molecule are listed. In addition, the

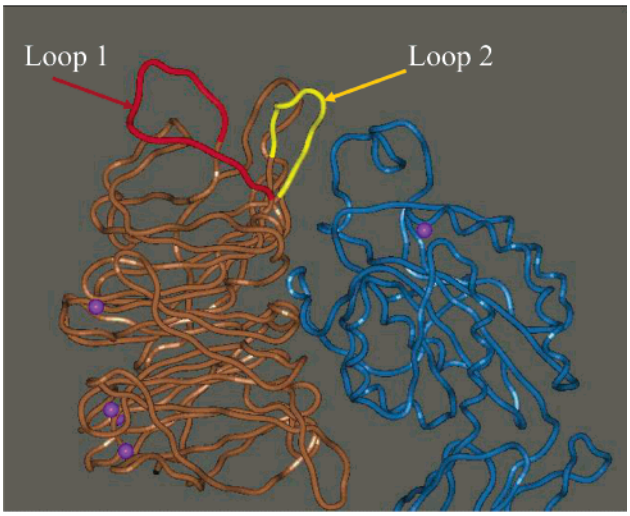

Figure 8. Final model of $\alpha_{IIb}\beta_3$. Loop 1 is shown in red and Loop 2 is in yellow.

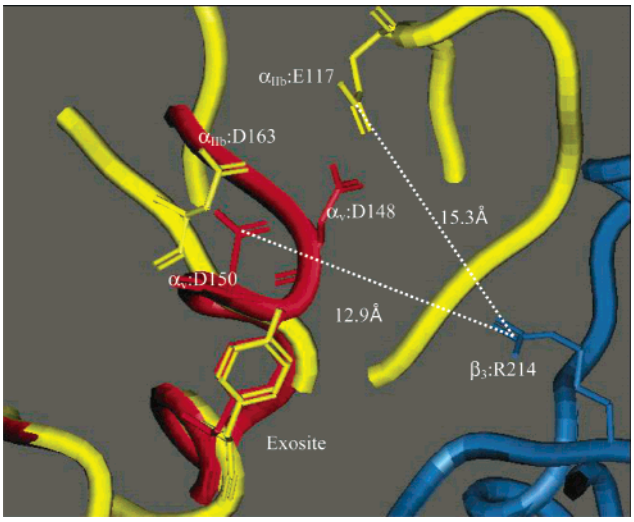

Figure 9. Comparison of the $\alpha_{IIb}\beta_3$ and $\alpha_v\beta_3$ binding site models, α_{IIb} is in yellow, α_v is in red and β_3 is in blue. Note the exosite (tyrosine) and the basic residue (β_3:R214) are in the same or nearly same relationship in both models. However, the important acidic residues have a greater separation distance in $\alpha_{IIb}\beta_3$ than in $\alpha_v\beta_3$ leading to specificity differences.

last two columns give the RMSD between the RBS and FBS with and without superposition. The ligand−protein interaction distances are listed in Table 5 for both the RBS and FBS models. Specifically, the distances between (i) the carbon of the ligand's carboxylic acid and the carbon of the guanidine group, (ii) the ligand's charged nitrogen and the carbon of the protein carboxylate, and (iii) the minimum distance between the ligand and Y190 are reported and also depicted in Figures 10−18.

The RMSD between the bound conformation and the closest in vacuo minimum is an indication of the internal strain of the molecule induced by the interaction with the protein. For the RBS, molecules **4**, **5**, **7**, and **8** have an RMSD above 1.0 Å indicative of the most induced strain. The remaining non-$\alpha_{IIb}\beta_3$ binders, **6** and **9**, have the low RMSDs, but **6** is a very rigid molecule and **9** does not make the exosite interaction as indicated in Table 5. Even though the dual antagonist, **4**, appears to have good interaction distances, it is found to have

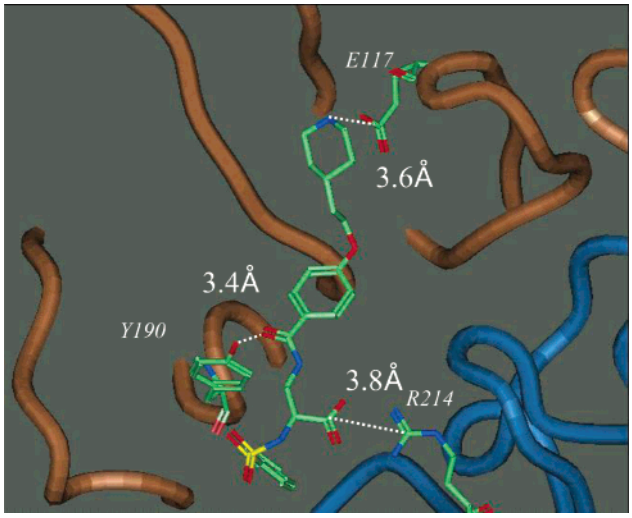

Figure 10. Binding model for **1**.

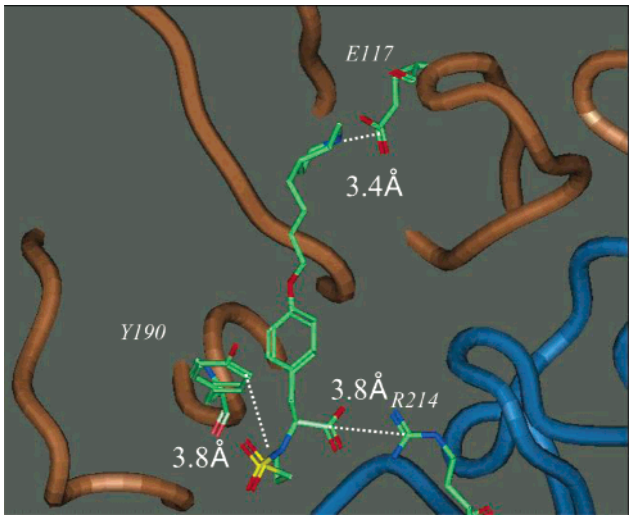

Figure 11. Binding model for **2**.

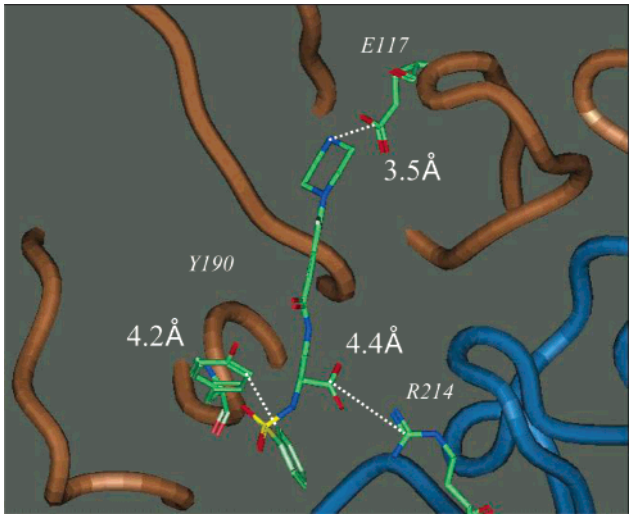

Figure 12. Binding model for **3**.

the most internal strain as indicated in Table 4. When relaxing the side-chains and ligands simultaneously, it is expected that more favorable and hence stronger electrostatic interactions will prevail as the charge groups optimize their separation distance. Subsequently, the binding will get stronger at the expense of

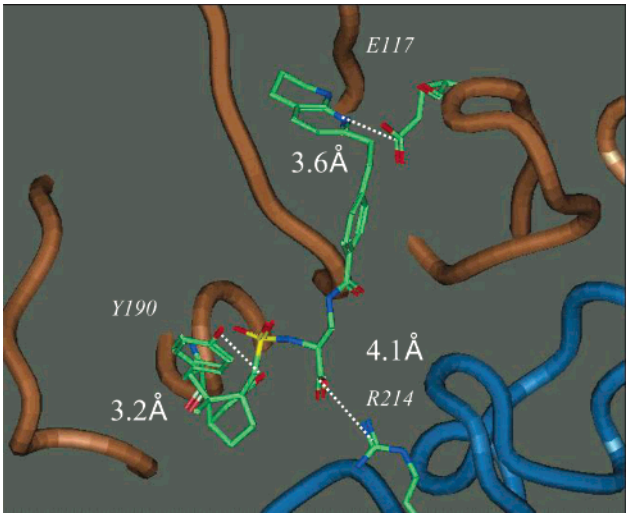

Figure 13. Binding model for **4**.

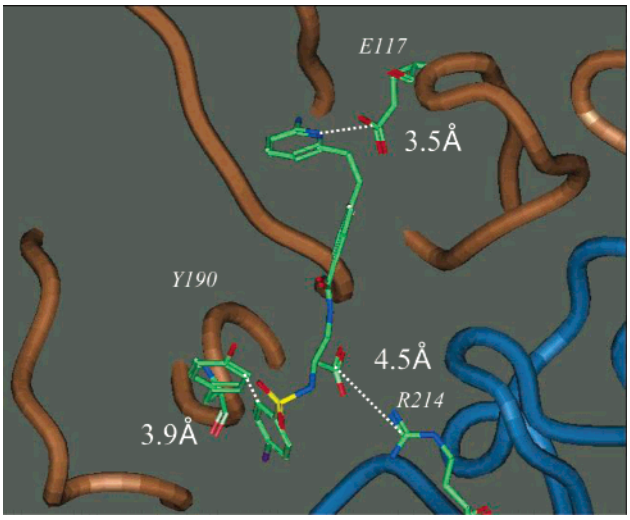

Figure 14. Binding model for **5**.

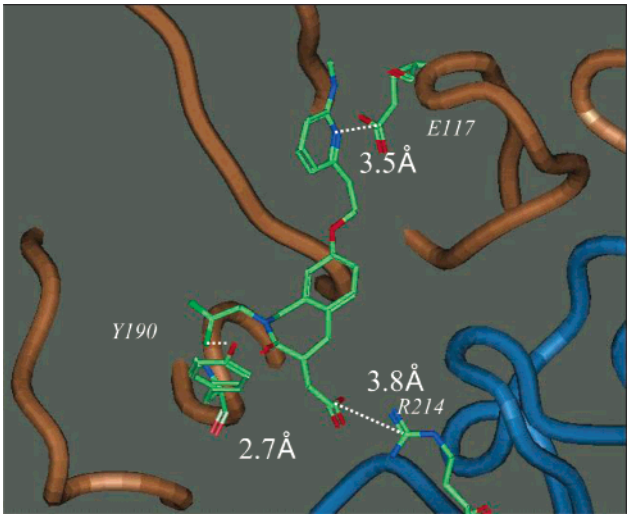

Figure 15. Binding model for **6**.

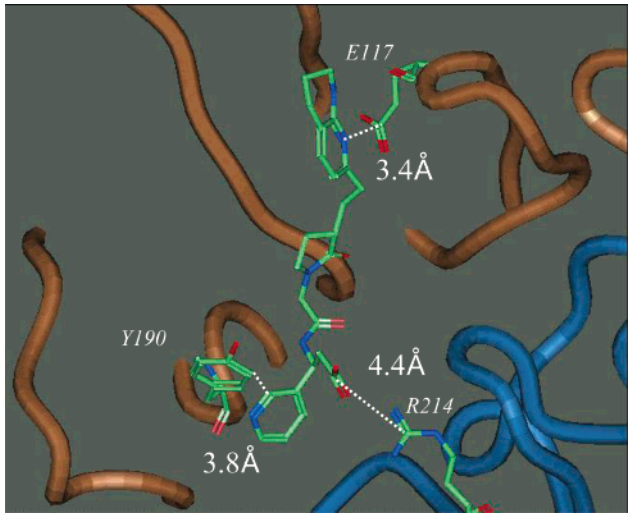

Figure 16. Binding model for **7**.

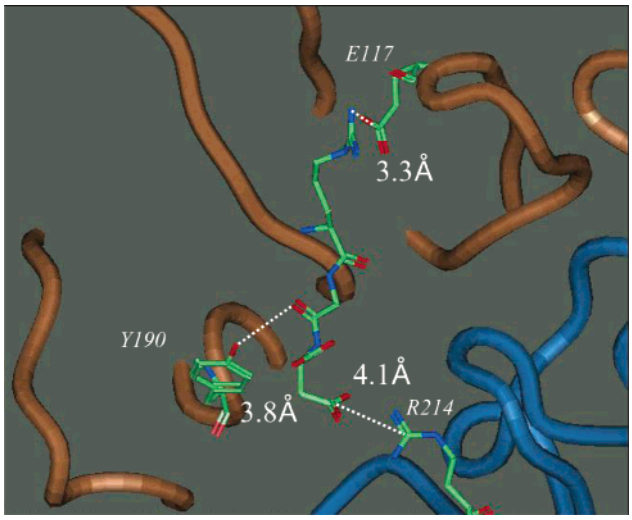

Figure 17. Binding model for **8**.

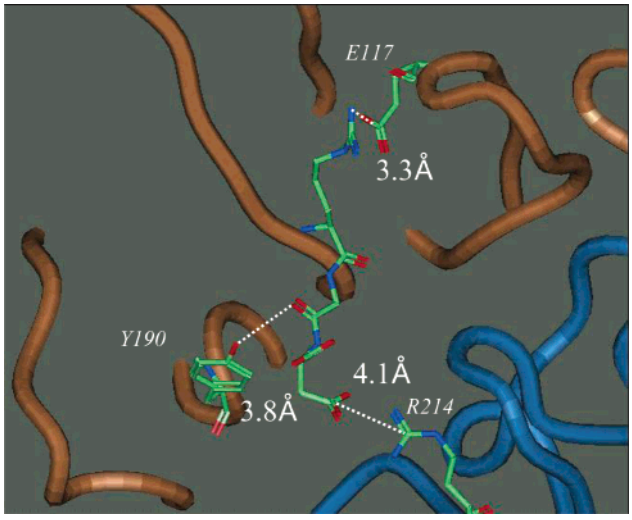

Figure 18. Binding model for **9**.

more strain in the ligand, as indicated by the increase in the FBS/E_0 RMSD (Table 4: column heading FBS/E_0). The exceptions to this general observation occur when the protein−ligand interactions change dramatically as in **4**, **6**, and **8**. Compound **4** finds a more favorable exosite interaction after relaxation, while both **6** and **8** completely lose the exosite interaction in favor of better charge interactions and less internal strain. Both of these latter two molecules also have the largest relative movement of the ligand during relaxation as seen in the last column of Table 4. It appears that **7** has obtained a good binding mode upon relaxation of

Table 4. Root-Mean-Square-Deviations (RMSD) between Bound Conformations and Conformation of Closest Energy Minimum

molecule ID	RMSD (Å): RBS/E_0	RMSD (Å): FBS/E_0	RMSD (Å): RBS/FBS	RMSD (Å): RBS/FBS absolute
1	0.88	1.19	0.84	1.35
2	0.90	0.93	0.79	1.59
3	0.39	0.52	0.70	1.62
4	1.90	1.84	0.66	1.80
5	1.22	1.31	0.74	0.83
6	0.85	0.74	0.25	1.96
7	1.21	1.58	0.88	1.23
8	1.55	0.93	1.25	3.25
9	0.50	1.59	1.62	1.95

[a] RS: ligand in rigid site, FS: ligand in flexible site, E_0: closest local minimum for neural molecule in vacuo. Absolute: RMSD between small-molecule conformations in rigid and relaxed protein without superposition.

Table 5. Important Protein−Small-Molecule Contact Distances

	contacts in rigid binding site			contacts in relaxed binding site		
molecule ID	COO to R214:CNN	N+ to E117:COO	minimum to Y190	COO to R214:CNN	N+ to E117:COO	minimum to Y190
1	3.8	3.6	3.4[a,b]	3.7	3.5	2.7[a,b]
2	3.8	3.4	3.8[c]	3.8	2.9	3.8[c]
3	4.4	3.5	4.2[a]	3.9	3.5	4.1[b]
4	4.1	3.6	3.2[b]	3.8	3.6	2.7[b]
5	4.5[5]	3.5	3.9[a]	4.0[e,f]	3.4	4.1[a]
6	3.8	3.5	2.7[b]	3.7	3.6	6.2[d]
7	4.4[5]	3.4	3.8[a]	3.7	3.5	2.9[b]
8	4.6[5]	3.4	3.3[b]	3.8[e]	4.2	6.7[d]
9	4.1	3.3	3.8[d]	3.7	3.4	4.1[d]

[a] $\pi-\pi$ stacking. [b] Hydrogen bond. [c] Hydrophobic. [d] No binding interaction. [e] Unfavorable orientation. [f] Shared interaction with β_3:R16.

the protein; however, as previously noted, the flexible binding mode of **7** has significant induced strain. It could be argued that a local minimum closer to the bound conformation was simply not generated when sampling conformational space. Although this may be the case, a visual inspection of Figures 10−18 depicts the bound conformation of the $\alpha_{IIb}\beta_3$ active compounds to be in a more favorable extended conformation than the inactives such as **7**. Even though **7** appears to make the necessary contacts, it does so at the expense of inducing considerable internal strain.

In addition to the distance between the functional groups, the relative orientation of the interacting groups is also important for binding. As seen in Figures 14, 16, and 17 and Table 4, the acidic moieties in **5**, **7**, and **8** have greater ligand−protein interaction distance and an unfavorable orientation compared to **1**−**3**. Compound **4**, a dual $\alpha_{IIb}\beta_3/\alpha_v\beta_3$ antagonist, falls between these two extremes as would be expected for a ligand 10-fold less active than the selective antagonists, **1**−**3**. Compound **4** achieves an acceptable interaction distance and orientation but only at cost of significant internal strain in both the RBS and FBS.

Similarly to the $\alpha_v\beta_3$ model, exosite binding involves a favorable interaction with a tyrosine residue, α_{IIb}:Y190, which may be characterized as $\pi-\pi$ stacking in the cases of **1** and **3**,[28] and a hydrophobic interaction with **2**. As indicated in Figure 1, mutation of α_{IIb}:Y190 negatively affects binding. The results for the FBS find three of five inactive compounds, **6**, **8**, and **9**, fail to achieve a favorable interaction with the exosite upon relaxation of the protein and ligand. While **5** and **7** exhibit exosite binding, **5** does not have a favorable β_3:R214 interaction and **7** is significantly strained.

Conclusions

A model of the $\alpha_{IIb}\beta_3$ integrin has been developed. The model was constructed from the $\alpha_v\beta_3$ crystal structure, a homology model for the α_{IIb} subunit and studies of small ligand binding. The conformations of the two important α_{IIb} loops, indeterminate from the homology model, were identified as key components for nonpeptide ligand binding. A thorough conformational search followed by local energy minimization yielded a number of potential models. The model most consistent with known SAR and mutagenesis experiments is reported here. The putative binding site of the $\alpha_{IIb}\beta_3$ integrin is similar to the recently published $\alpha_v\beta_3$ model complete with an exosite interaction involving α_{IIb}:Y190. The model provides a rational explanation of the differences in observed activity of the nine compounds studied, three $\alpha_{IIb}\beta_3$ selective antagonists, one $\alpha_{IIb}\beta_3/\alpha_v\beta_3$ dual antagonist, four $\alpha_v\beta_3$ selective antagonists, and a compound inactive for both integrins. The primary explanation for the different assay results of the ligands is the greater distance between the charged residues of the binding site of the $\alpha_{IIb}\beta_3$ protein versus $\alpha_v\beta_3$ while maintaining the same exosite/β_3 relationship.

Acknowledgment. The authors would like to thank the Merck West Point medicinal chemists and biologists who devoted so much time and effort to understanding and controlling the action of integrins, especially Drs. P. Coleman, M. Duggan, L. Duong, M. Egbertson, J. Hutchinson, R. Meissner, G. Rodan, and S. Rodan. The technical assistance of Dr. V. Maiorov in obtaining Ramachandran plots is also gratefully acknowledged.

Supporting Information Available: The complete PDB structure file of the $\alpha_{IIb}\beta_3$ model.

References

(1) Curley, G. P.; Blum, H.; Humphries, M. J. Integrin antagonists. *Cell Mol. Life Sci.* **1999**, *56*, 427−441.
(2) Coller, B. S. Perspective Series: Cell adhesion in vascular biology. *J. Clin. Invest.* **1997**, *99*, 1467−1471.

(3) Scarborough, R. M.; Gretler, D. D. Platelet Glycoprotein IIb-IIIa Antagonists as Prototypical Integrin Blockers: Novel Parenteral and Potential Oral Antithrombotic Agents. *J. Med. Chem*. **2000**, *43*, 3453−3473.
(4) Duong, L. T.; Rodan, G. A. Regulation of osteoclast formation and function. *Rev. Endo. Metab. Dis*. **2001**, *2*, 95−104
(5) Humphries, M. J. Integrin Structure. *Biochem. Soc. Trans*. **2002**, *28*, 311−339.
(6) Adair, B. D.; Yeager, M. Three-dimensional Model of the human platelet integrin αIIbβ3 based upon electron cryomicroscopy and X-ray crystallography. *Proc. Natl. Acad. Sci. U.S.A*. **2002**, *99*, 14059−14064.
(7) Lee, J. O.; Rieu, P.; Arnaout, M. A.; Liddington, R. Crystal structure of the A domain from the alpha subunit of integrin CR3 (CD11b/CD18). *Cell* **1995**, *80*, 631−638.
(8) Michishita, M.; Videm, V.; Arnaout, M. A. A novel divalent cation-binding site in the A domain of the beta 2 integrin CR3 (CD11b/CD18) is essential for ligand binding. *Cell* **1993**, *72*, 857−867.
(9) Loftus, J. C.; O'Toole, T. E.; Plow, E. F.; Glass, A.; Frelinger, A. L., III; Ginsberg, M. H. A beta 3 integrin mutation abolishes ligand binding and alters divalent cation-dependent conformation. *Science* **1990**, *249*, 915−918.
(10) PDB ID: 1JV2. Xiong, J.-P.; Stehe, T.; Diefenbach, B.; Zhang, R.; Dunker, R.; Scott, D. L.; Joachimiak, A.; Goodman, S. L.; Arnaout, M. A. Crystal Structure of the Extracellular Segment of Integrin αVβ3. *Science* **2001**, *294*, 339−345.
(11) Pfaff, M.; Tangemann, K.; Muller, B.; Gurrath, M.; Muller, G.; Kessler, H.; Timpl, R.; Engel, J. Selective Recognition of Cyclic RGD Peptides of NMR Defined Conformation by αIIbβ3, αVβ3 and α5β1 Integrins. *J. Biol. Chem*. **1994**, *269*, 20233−20238.
(12) Hartman, G. D.; Egbertson, M. S.; Halczenko, W.; Laswell, W.; Duggan, M. E.; Smith, R. L.; Naylor, A. M.; Manno, P. D.; Lynch, R. J.; Zhang, G.; Chang, C. T.-C.; Gould, R. L. Nonpeptide Fibrinogen Receptor Antagonists. 1. Discovery And Design of Exosite Inhibitors. *J. Med. Chem*. **1992**, *35*, 4640−4642.
(13) Askew, B. C.; Bednar, R. A.; Bednar, B.; Claremon, D. A.; Cook, J. J.; McIntyre, C. J.; Hunt, C. A.; Gould, R. J.; Lynch, R. J.; Lynch, J. J.; Gaul, S. L.; Stranieri, M. T.; Sitko, G. R.; Holahan, M. A.; Glass, J. D.; Hamill, T.; Gorham, L. M.; Prueksaritanont, T.; Baldwin, J. J.; Hartman, G. D. Non-Peptide Glycoprotein IIb/IIIa INhibitors. 17. Design And Synthesis Of Orally Active, Long-acting Non-peptide Fibrinogen Receptor Antagonists. *J. Med. Chem*. **1997**, *40*, 1779−1788.
(14) Hartman, G. D.; Duggan, M. E.; Hoffman, W. F.; Meissner, R. S.; Perkins, J. J.; Zartman, A. E.; Naylor-Olsen, A.; Cook, J. J.; Glass, J.; Lynch, R. J.; Zhang, G.; Gould, R. Nonpeptide Glycoprotein IIB/IIIA Inhibitors. 19. A new Design papradigm employing linearly minimized, centrally constrained, exosite inhibitors. *Bioorg. Med. Chem. Lett*. **1999**, *9*, 863−868.
(15) Feuston, B. P.; Culberson, J. C.; Duggan, M. E.; Hartman, G. D.; Leu, C.-T.; Rodan, S. B. Binding model for nonopeptide antagonists of $\alpha_v\beta_3$ integrin. *J. Med. Chem*. **2002**, *45*, 5640−5648.
(16) Duggan, M. E.; Duong, L. T.; Fisher, J. E.; Hamill, T. G.; Hoffman, W. F.; Huff, J. R.; Ihle, N. C.; Leu, C.-T.; Nagy, R. M.; Perkins, J. J.; Rodan, S. B.; Wesolowski, G.; Whitman, D. B.; Zartman, A. E.; Rodan, G. A.; Hartman, G. D. Nonpeptide $\alpha_v\beta_3$ Antagonist. 1. Transformation of a Potent, Integrin-Selective $\alpha_{IIb}\beta_3$ Antagonist into a Potent $\alpha_v\beta_3$ Antagonist. *J. Med. Chem*. **2000**, *43*, 3736−3745.
(17) Meissner, R. S.; Perkins, J. J.; Duong, L. T.; Hartman, G. D.; Hoffman, W. F.; Huff, J. R.; Ihle, N. C.; Leu, C.-T.; Nagy, R. M.; Naylor-Olsen, A.; Rodan, G. A.; Rodan, S. B.; Whitman, D. B.; Wesolowski, G.; Duggan, M. E. Nonpeptide $\alpha_v\beta_3$ Antagonist. 2. Constrained Glycyl Amides Derived From RGD Tripeptide. *Bioorg. Med. Chem. Lett*. **2002**, *12*, 25−29.
(18) Coleman, P. J.; Brashear, K. M.; Hunt, C. A.; Hoffman, W. F.; Hutchinson, J.; Breslin, M. J.; McVean, C. A.; Askew, B. C.; Hartman, G. D.; Rodan, S. B.; Rodan, G. A.; Leu, C.-T.; Prueksaritanont, T.; Fernandez-Metzler, C.; Ma, B.; Libby, L. A.; Merkle, K. M.; Stump, G. L.; Wallace, A. A.; Lynch, J. J.; Lynch, R.; Duggan, M. E. Non-Peptide $\alpha_v\beta_3$ Antagonists. Part III: Identification of Potent RGD Mimetics Incorporating Novel β-Amino Acids as Aspartic Acid Replacements. *Bioorg. Med. Chem. Lett*. **2002**, *12*, 31−34
(19) Duggan, M. E. Preparation of heterocyclic peptide derivatives as integrin antagonists. *PCT Int. Appl*.; Merck & Co., Inc.: USA, 1998; p 74.
(20) Coleman, P. J.; Askew, B. C.; Hutchinson, J.; Whitman, D. B.; Perkins, J. J.; Hartman, G. D.; Rodan, G. A.; Leu, C.-T.; Prueksaritanont, T.; Fernandez-Metzler, C.; Merkle, K. M.; Lynch, R.; Lynch, J. J.; Rodan, S. B.; Duggan, M. E. Non-Peptide $\alpha_v\beta_3$ Antagonists. Part 4: Potent and Orally Bioavailable Chain Shortened RGD Mimietics. *Bioorg. Med. Chem. Lett*. **2002**, *12*, 2463−2465.
(21) PDB ID: 1JX5. Kamata, T.; Tieu, K. K.; Irie, A.; Springer, T. A.; Takada, Y. Amino acid residues in the alpha(IIb) subunit that are critical for ligand binding to integrin alpha(IIb)beta(3) are clustered in the beta-propeller model. *J. Biol. Chem*. **2001**, *276*, 44275−44283.
(22) Chemical Computing Group, v.2000.02, 1010 Sherbrooke Street West, Suite 910, Montreal, Quebec, Canada H3A 2R7.
(23) BatchMin and MacroModel were developed in the laboratories of Professor Clark Still (Columbia University) and are available from Schrodinger, Inc. (Portland, OR). Version 5.0 was released in 1995.
(24) Halgren, T. A. Merck Molecular Force Field. I Basis, Form, Scope, Parameterization, and Performance of MMFF94. *J. Comp Chem*. **1996**, *17*, 490−519.
(25) Yamamoto, M.; Fisher, J. E.; Gentile, M.; Seedor, J. G.; Leu, C.-T.; Rodan, S. B.; Rodan, G. A. The integrin ligand echistatin prevents bone loss in ovariectomized mice and rats. *Endocrinology* **1998**, *139*, 1411−1419.
(26) Badger, A. M.; Blake, S.; Kapadia, R.; Sarkar, S.; Levin, J.; Swift, B. A.; Hoffman, S. J.; Stroup, G. W.; Miller, W. H.; Gowen, M.; Lark, M. W. Disease-Modifying Activity of SB273005, an Orally Active, Nonpeptide $\alpha_v\beta_3$ (Vitronectin Receptor) Antagonist, in Rat Adjuvant-Induced Arthritis. *Arthritis Rheum*. **2001**, *44*, 128−137.
(27) Feuston, B. P.; Miller, M. D.; Culberson, J. C.; Nachbar, R. B.; Kearsley, S. K. Comparison of Knowledge-Based and Distance Geometry Approaches for Generation of Molecular Conformations. *J. Chem. Inf. Comput. Sci*. **2001**, *41*, 754−763.
(28) Hunter, C. A.; Sanders, J. K. M. The Nature of $\pi-\pi$ Interactions. *J. Am. Chem. Soc*. **1990**, *112*, 5525−5534.

JM030146J